Dependence between Ionic Liquid Structure and Mechanism of Visible-Light-Induced Activity of TiO2 Obtained by Ionic-Liquid Assisted Solvothermal Synthesis

Ionic liquid-assisted synthesis of visible light active N-doped TiO_2 photocatalysts

Marta Paszkiewicz-Gawron[a], Marta Długokęcka[b], Wojciech Lisowski[c], Elio Giamello[d], Tomasz Klimczuk[e], Ewelina Grabowska[a], Adriana Zaleska-Medynska[a], Justyna Łuczak[b]

[a]*Department of Environmental Technology, Faculty of Chemistry, University of Gdansk, Wita Stwosza 63, 80-308 Gdansk, Poland*
[b]*Department of Chemical Technology, Faculty of Chemistry, Gdansk University of Technology, G. Narutowicza 11/12, 80-233 Gdansk, Poland*
[c]*Institute of Physical Chemistry, Polish Academy of Sciences, Kasprzaka 44/52, 01-224 Warsaw, Poland*
[d]*Department of Chemistry and NIS Interdepartmental Centre, University of Turin, Via P. Giuria 7, I-10125 Torino. Italy*
[e]*Department of Solid State Physics, Faculty of Applied Physics and Mathematics, Gdansk University of Technology, 80-233 Gdansk, Poland*

1. Abstract:

Four ionic liquids (ILs), all based on distinct, nitrogen containing, cations were selected for IL-TiO_2 composites preparation and investigation of the effect of IL structure on morphology and performance under visible irradiation of the IL-TiO_2 photocatalysts. Application of the selected ionic liquids allowed to receive materials capable to use visible photons, beside UV ones, for the promotion of electrons in the conduction band, thus formation highly active photocatalysts. The sample that exhibited the highest photoactivity under Vis irradiation (58%) was TiO_2 prepared in a presence of 1-butylpyridinium chloride with 1:3 (precursor: IL) molar ratio. The comparative approach revealed that the amount of IL (molar ratio of TBOT:IL used for synthesis) needed to obtain IL-TiO_2 sample with the highest photoactivity differed for various IL structures. Therefore, this parameter should be taken onto account when procedures for preparation of TiO_2 particles with the expected properties are designed. Based on the extensive characteristics (SEM, XRD, XPS etc.), the successful modification of the TiO_2 with IL species including possible interactions between the IL and TiO_2 surface as well as TiO_2 matrix (Ti-N_x) were confirmed. The effect of the IL's structure on the visible light-induced photoactivity of the IL-TiO_2 was presented and discussed in regard to structure, morphology, absorption properties, elemental composition of particles, and the reactive species involved in the photocatalytic reaction of phenol degradation. Electron paramagnetic resonance technique revealed that the superoxide radical species $O_2^{\bullet -}$ where the main active species responsible for high efficiency of phenol degradation. Additionally, the photoluminescence experiments implied that the presence of ILs effectively improved the inhibition of electron and electron-hole recombination. In this regard, the IL-TiO_2 photocatalysts meet the specifications for use in various photocatalytic applications due to their large surface area and high activity in visible light.

Keywords: ionic liquids, titanium dioxide, solvothermal method, heterogeneous photocatalysis, active species, nitrogen doping

2. Introduction

TiO_2 photocatalysts are the most commonly-used semiconductor materials for environmental applications such as air/water purification, wastewater treatment, bacteria inactivation and water splitting [1]. However, the practical application of TiO_2 has been impeded by its low efficiency for utilizing solar energy and its low quantum yield resulting from its wide band gap and high recombination rate of photogenerated charge carriers [2]. It is known that the performance and thus the applications of TiO_2 are strongly dependent on its own crystalline structure, morphology (exposed crystal faces, shape and pore volume and structure) and size of the particles. Therefore, to enhance the activity and widespread the application of TiO_2 photocatalysis studies are focused on the adjusting and control of these factors [3]. Additionally, the microstructure and electronic structure, surface properties, and the photoactivity of TiO_2 are largely dependent on the synthesis conditions and procedures. For instance, the hydro- and solvothermal methods have been widely used due to their simplicity and short reaction time.

Very recently, ionic liquids (ILs) have been used in preparation of TiO_2 particles serving as (co-)solvents [4-6], templating agents [7-10], capping/morphology-controlling agents [5, 11, 12] and microwave absorbers [13-16]. Among the main advantages of using ILs as solvents is their polarity that is higher than most of the molecular solvents and determine solubility of the reagents [17]. Additionally, the higher viscosity of the ILs, in comparison to water or classical organic solvents, decreases the particles aggregation rate and affects heat and mass transport, hence reaction rate and selectivity [18]. ILs have been used as structure formatting agents (templating and capping agents) due to their amphiphilicity [19], thus structural organization through self-assembly, and tunable properties, therefore ability for controlling the nucleation and growth kinetics in manipulating the size and shape of the nano- and microstructures [9]. Latterly, it was observed that ILs introduced during synthesis can interact with TiO_2 surface resulting in enhancement of UV or visible light response of semiconductor [12, 16, 20]. Surface modified TiO_2 nanocomposites by 1-buthyl-3-methylimidazolium hydroxide [BMIM][OH] ionic liquid, synthesized by hydrothermal method, shows a red-shifted optical response [21]. Moreover, the highest occupied molecular orbital (HOMO) and the lowest unoccupied molecular orbital (LUMO) of [BMIM][OH] match well with the conduction band (CB) and valence band (VB) of TiO_2, leading to improved photocatalytic activity under visible light for the degradation of methylene blue. Zhong et al revealed that the addition of 1-butyl-3-methylimidazolium hexafluorophosphate [BMIM][PF_6] during the synthesis of TiO_2 has a strong effect on the transport properties of the photogenerated charges as well as it increases the hydroxyl content on the surface of the photocatalysts. However, it is not clear at this moment which element (F, P or together) or structural changes caused this difference [22]. Jing et al. synthesized TiO_2 modified by 1-allyl-3-(butyl-4-sulfonyl)imidazolium hydrosulfate [ABsIM][HSO_4], which showed prominent photoelectrochemical water oxidation performance, exhibiting a ten-fold photocurrent compared to the unmodified TiO_2 under the same conditions [23]. Furthermore, long-term PEC water splitting processes proved that the photo-stability of IL-TiO_2 was greatly enhanced with respect to the unmodified solid. The significantly enhanced PEC performance of IL-TiO_2 was ascribed to a synergistic effect between covalently linked IL units and TiO_2 particles. Qi et al. found that the addition of 1-butyl-3-methylimidazolium tetrafluoroborate [BMIM][BF_4] can enhance or suppress the photocatalytic degradation of methyl orange (MO) or rhodamine B (RhB), respectively, depending on the trapping and transfer of the photogenerated electrons and holes [24]. For the MO photocatalytic reaction, photoefficiency increased because adsorption of [BMIM] ions on the surface of TiO_2 can enhance trapping and transfer of the photogenerated electrons, as well as facilitate adsorption of MO due to the electrostatic attraction between positively charged [BMIM] ions and negatively charged MO in the solution. On the contrary, during RhB

degradation, addition of IL suppressed the photodegradation because [BMIM] on the surface of TiO_2 hinders the access of positively charged RhB to the surface of TiO_2 and also restricts the diffusion of positively charged holes to the TiO_2/solution interface due to the electrostatic repulsion between [BMIM] and holes. Improvement of photocatalytic activity of IL-assisted TiO_2 was also ascribed to doping of titania by IL-building elements. For instance, N, C and F codoped rutile titania nanorods were prepared in the presence of [BMIM][BF_4] and showed a remarkable improvement in photocatalytic degradation of Congo red under visible light irradiation [7]. Also Yu *et al*. used [BMIM][BF_4] as a dopant source of F, B and C for the synthesis of fluorinated B, C codoped anatase TiO_2 *via* the hydrothermal method [25]. Based on the literature data, it could be stated that ILs introduced during the synthesis route could improve visible light response of wide band gap semiconductors (e.g. TiO_2) due to: (i) doping of TiO_2 by non-metal elements constituting ILs (such as C, F, P, B) [7, 25, 26]; (ii) direct sensibilization of TiO_2 [10]; (iii) surface complex charge transfer [27]; (iv) favoring oxygen vacancies and Ti^{3+} species formation during synthesis [16]; (v) stimulating of hydroxyl group formation at the surface of metal oxide [x]; and (vi) affecting transport of photogenerated charges [24]. Notwithstanding, it is not clear at this moment how to correlate the structure of ILs and preparation conditions with the above mentioned factors. Moreover, in most cases photocatalytic activity of TiO_2 obtained *via* ILs-assisted preparation route are estimated in UV mediated reaction or using dyes as model compounds. This fact makes mechanism interpretation more difficult due to sensitization ability of dyes [2]. What is more, active species involved in the photodegradation reactions were rarely investigated.

In view of this, in this work, we present the synthesis of TiO_2 by an ionic liquid-assisted hydrothermal method and show the effect of the IL's cation type and IL content on the morphology, surface properties and photoactivity of TiO_2 microparticles. Four ILs, all based on chloride anions and on a series of distinct, nitrogen containing, cations (namely: 1-benzyl-3-methylimidazolium [BenMIM], 1-butylpyridinium [BPy], 1-butyl-1-methylpyrrolidinium [BMPyr] and tetrabutylammonium [TBA]) were selected for investigations the influence of ILs on semiconductor properties (Figure 1). These four ILs were selected since they are composed of cations with different structure, however all containing nitrogen atom(s). As a consequence, HOMO and LUMO energies of these salts differ significantly, being much lower (as observed for [BPy][Cl]) or similar ([TBA][Cl]) to titania band gap. To confirm the IL-TiO_2 composites formation, to describe the structure of the IL at the TiO_2 surface and to verify doping of IL's elements in the titania bulk structure the elemental analysis of the photocatalysts was performed. The photocatalytic activities of the as-obtained TiO_2 materials were evaluated by the degradation of phenol under visible light irradiation. To provide insight into the oxidative species participating in the degradation mechanism, electron paramagnetic resonance spectroscopy was employed. Moreover, the role of the active species in the process of the degradation was evaluated by using different types of active species scavengers. To support understanding of interactions between IL and TiO_2 NTs surface quantum chemical calculations at DFT level were performed.

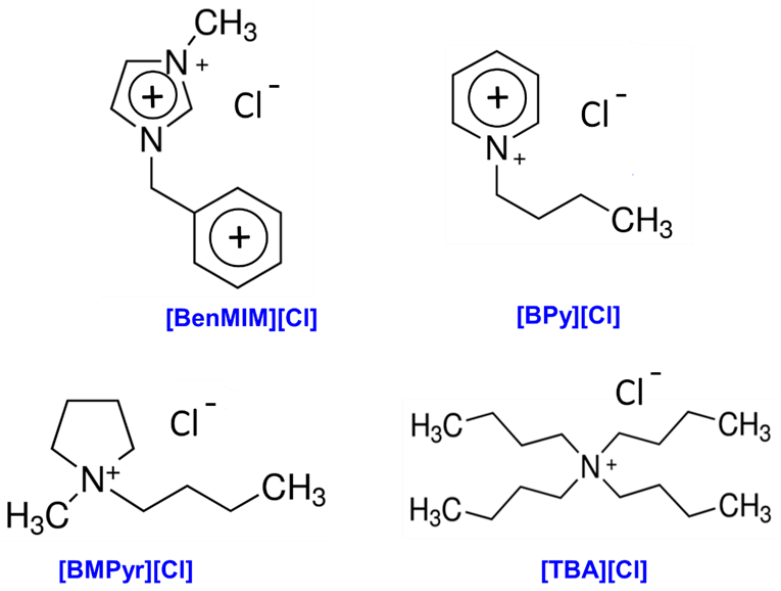

Figure 1. The structure of ionic liquids used during the synthesis: 1-benzyl-3-methylimidazolium chloride [BenMIM][Cl], 1-butylpyridinium chloride [BPy][Cl], 1-butyl-1-metylpyrrolidinium chloride [BMPyr][Cl] and tetrabutylammonium chloride [TBA][Cl]

3. Experimental

3.1 Preparation of IL-assisted TiO_2 particles

Titanium (IV) n-butoxide (TBOT, Sigma Aldrich) was dissolved in absolute ethanol (Sigma Aldrich), then HCl (Sigma Aldrich), distilled water and IL were added. The selected molar ratios of ILs to TBOT (IL:TBOT) are listed in Table 1. Four ILs, that are 1-benzyl-3-methylimidazolium chloride [BenMIM][Cl], 1-butylpyridinium chloride [BPy][Cl], 1-butyl-1-methylpyrrolidinium chloride [BMPyr][Cl] and tetrabutylammonium chloride [TBA][Cl] with purities of ≥ 99%, were purchased from Sigma Aldrich. The solvothermal reaction was performed in a 200 ml Teflon-lined stainless steel autoclave at 180°C for 24 h [12]. When the reaction was completed, the autoclave was cooled to room temperature, and the product was washed with ethanol, deionized water and dried at 50°C for 6 h. As prepared samples were calcined for 2 h in 200°C.

3.2 Characterization of IL-assisted TiO_2 particles

Powder X-ray diffraction (PXRD) measurements were conducted using Philips/PANalytical X'Pert Pro MPD diffractometer (PANalytical, Almelo, the Netherlands) with Cu-Kα radiation. The freshly grinded powder was homogeneously spread on the micro cover glass holder of ca. 0.2 mm depth. The PXRD data were processed by means of LeBail analysis using HighScore Plus software. The morphology and size distribution of the IL-TiO_2 samples were observed by scanning electron microscope (SEM), Hitachi Microscope TM-1000, under high vacuum with an accelerating voltage 15 kV. BET surface area and pore size of the photocatalysts (physical adsorption and desorption of nitrogen at 77 K) was measured by Micromeritics Gemini V200 Shimadzu instrument equipped in the VacPrep 061 Degasser. A Nicolet Evolution 220 UV-Vis spectrophotometer (Thermo) was used for obtain the diffuse reflectance UV-Vis absorption spectra of the samples, for which the baseline was a barium sulfate. A Thermo Scientific Flash 2000 CHNS analyzer was used to determine the elemental composition of the synthesized materials. X-ray photoelectron spectroscopy (XPS) experiments were performed

on a PHI 5000 VersaProbeTM (ULVAC-PHI) spectrometer with monochromatic Al Kα radiation (hν = 1486.6 eV). The X-ray beam was focused to a diameter of 100 μm, and the measured area was defined as a 250 μm square. The high-resolution (HR) XPS spectra were collected by the hemispherical analyzer at a pass energy of 23.5 eV, an energy step size of 0.1 eV and a photoelectron take off angle of 45° with respect to the surface plane. CasaXPS software was used to evaluate the XPS data. The HR XPS spectra were deconvoluted using a Shirley background and a Gaussian peak shape with 30% Lorentzian character. The binding energy (BE) scale of all detected spectra was referenced to the Ti $2p_{3/2}$ core level (BE=458.6 eV). Infrared spectra of the semiconductors were recorded on a Nicolet iS10 using Fourier transform infrared (FTIR) spectrometer (Thermo Scientific, USA) using a diffuse reflectance technique at a resolution of 8 cm^{-1} in the spectral range from 650 to 4000 cm^{-1}.

3.3 Measurement of photocatalytic activity

3.3.1 Phenol degradation under Vis irradiation

The photocatalyst (0.125 g) was dispersed in 25 ml of a phenol solution (0.21 mmol/dm^3) in a cylindrical reactor with quartz window (aeration - 5 dm^3/h; temperature of water bath was 10 ± 0.5°C; 1000 W Xenon lamp, 6271H Oriel; optical filter >420 nm, GG 420). The phenol concentration was determined by colorimetric method (λmax = 480 nm) using UV-Vis spectrophotometer (Evolution 220, Thermo-Scientific). The photocatalytic degradation runs were preceded by a blind test in the absence of photocatalysts or illumination. No phenol degradation was observed in the absence of illumination.

3.3.2 Experiments with trapping agents

Controlled photoactivity experiments under Vis radiation were carried out using different scavengers (ammonium oxalate as a scavenger of photogenerated holes, $AgNO_3$ for electrons, benzoquinone for superoxide radical species, and tert-butyl alcohol for hydroxyl radical species). The scavenger concentration was equal to the phenol content, and experiments were performed analogously to the photocatalytic degradation of phenol described above, except that the scavengers were added to the reaction system.

3.3.3 Electron paramagnetic resonance (EPR) measurements

For the spectroscopic characterization of all the samples a quartz tubular cell allowing treatments under vacuum and *in situ* EPR measurements was employed. X-band CW-EPR spectra were detected at 77 K on a Bruker EMX spectrometer (microwave frequency 9.46 GHz) equipped with a cylindrical cavity. A microwave power of 1 mW, a modulation amplitude of 0.2 mT and a modulation frequency of 100 KHz were used.

4. Results and discussion

To investigate the effect of selected ILs on the improvement of visible light induced photoactivity, mechanism of phenol degradation as well as active species involved in this process twenty four IL-TiO_2 photocatalysts were prepared using four ILs with various molar ratios of IL to Ti precursor (IL:TBOT): 10:1; 1:8; 5:1; 1:3; 1:2 and 1:1 (Table 1). This mode of action let us to select proper IL:TBOT molar ratio that enable to obtain the photocatalyst with the highest photoactivity under visible radiation for specific IL. The selected photocatalysts were subsequently characterized taking into account surface and optical properties; elemental composition, thereby interactions between IL and TiO_2. Finally, photocatalytic performance accompanied by active species responsible for visible light

activity were determined. This thorough characteristics let us to conclude about mechanism and the role of IL of photocatalytic improvement under visible irradiation.

Table 1. Sample label, applied ions, molar ratio of reagents (IL:TBOT), surface properties and photoactivity under visible irradiation of IL-assisted TiO_2

Sample label	Cation of ionic liquid	Anion of ionic liquid	Molar ratio (IL:TBOT)	Specific surface area ($m^2 \cdot g^{-1}$)	Pore volume ($cm^3 \cdot g^{-1}$)	Phenol degradation reaction rate under Vis irradiation (%)
TiO_2	-	-	-	184	0.069	13
TiO_2_BenMIM(1:10)	[BenMIM]	[Cl]	1:10	223	0.109	34
TiO_2_BenMIM(1:8)			1:8	191	0.094	19
TiO_2_BenMIM(1:5)			1:5	212	0.104	31
TiO_2_BenMIM(1:3)			1:3	183	0.090	13
TiO_2_BenMIM(1:2)			1:2	207	0.101	44
TiO_2_BenMIM(1:1)			1:1	170	0.083	15
TiO_2_BPy(1:10)	[BPy]	[Cl]	1:10	213	0.104	22
TiO_2_BPy(1:8)			1:8	214	0.104	18
TiO_2_BPy(1:5)			1:5	213	0.104	45
TiO_2_BPy(1:3)			1:3	215	0.105	58
TiO_2_BPy(1:2)			1:2	208	0.102	53
TiO_2_BPy(1:1)			1:1	198	0.097	34
TiO_2_BMPyr(1:10)	[BMPyr]	[Cl]	1:10	197	0.097	26
TiO_2_BMPyr(1:8)			1:8	209	0.103	49
TiO_2_BMPyr(1:5)			1:5	213	0.104	49
TiO_2_BMPyr(1:3)			1:3	228	0.111	33
TiO_2_BMPyr(1:2)			1:2	228	0.111	25
TiO_2_BMPyr(1:1)			1:1	217	0.110	20
TiO_2_TBA(1:10)	[TBA]	[Cl]	1:10	172	0.083	38
TiO_2_TBA(1:8)			1:8	210	0.102	22
TiO_2_TBA(1:5)			1:5	207	0.101	39
TiO_2_TBA(1:3)			1:3	208	0.101	41
TiO_2_TBA(1:2)			1:2	209	0.102	46
TiO_2_TBA(1:1)			1:1	202	0.100	23

4.1 Photocatalytic activity

The photocatalytic efficiency of the IL-assisted samples was estimated using aqueous solution of phenol as a model contaminate. Phenol was chosen due to high toxicity and no absorption in the visible spectrum in contrast to organic dyes (Rhodamine B, methylene blue) often used as model contaminations in the photocatalytic activity experiments [28]. The photocatalytic activity of IL-TiO_2 semiconductors under visible irradiation (optical filter >420 nm) is shown in Table 1. It was found that amount of IL (molar ratio of TBOT:IL used for synthesis) needed to obtain IL-TiO_2 samples with the highest photoactivity is not constant and differed for various IL structures. Moreover, the type of IL also affected their photoactivity. The highest degradation efficiency of phenol was revealed for TiO_2 samples obtained in a presence of [BPy][Cl] followed by [BMPyr][Cl]. For entire series containing [BPy][Cl] photodegradation efficiency of as-prepared samples increased with increasing quantity of IL up to molar ratio of 1:3. The ability of pollutant degradation increased from 13% determined for reference TiO_2 to 58% for TiO_2_BPy(1:3) sample and was accompanied by rise of specific surface area (up to 215 $m^2 \cdot g^{-1}$). Analogous observations were made for the other ILs. Hence, the highest terminal IL:TBOT ratios which determine improvement of the photocatalytic activity were TiO_2_BenMIM(1:2); TiO_2_BMPyr(1:5); TiO_2_TBA(1:2), respectively. In this regard, higher photocatalytic activity of these samples can be explained in terms of their larger surface area (Table 1). This, in turn, may provide more active sites and shorten the bulk diffusion length of charge carriers, thus suppressing bulk recombination [16].
What is interesting, further increase of the IL taken to the synthesis resulted in the opposite effect in case of both surface area and photoactivity. Decrease in photocatalytic efficiency is consistent with results of Chen [16] and Li [29], who investigated effect of [BMIM][BF_4] on TiO_2 obtained by microwave-assisted solvothermal reaction as well as our previous results obtained for 1-alkyl-3-methylimidazolium chlorides [12] and 1-butyl-3-methylimidazolium bromides, hexafluorophosphates and octylsulphates [27]. Li et al. proposed that lower TiO_2 photoactivity in the presence of excess of IL is related with N, B and F elements which become the recombination centers of the photo-induced electrons and holes [29]. In general for all series of samples the similar effect was observed (Table 1). To correlate the structure of IL cation with ILs-TiO_2 visible light induced photoactivity, only samples showing the highest photoactivity were chosen for further characterization.

4.2 Structure, morphology and absorption properties characterization

The ambient temperature powder diffraction patterns (PXRD) for four selected for further testing IL-TiO_2 and reference TiO_2 samples are shown in Figure 2. The experimental data are represented by points, whereas a red line is a LeBail fit to the data. Expected Bragg reflections for TiO_2 – anatase model, are shown by vertical bars. PXRD confirms high quality anatase (no impurities found) of our samples. The diffraction reflections are broad due to small crystallite size that was estimated from the Scherrer formula based on the basis of the (101) reflection width. These observations are in agreement with the results presented in our previous study [12]. The IL-TiO_2 samples prepared under the same conditions possessed analogous crystallinity, while shortening of the reaction time as well as lowering of temperature resulted in incomplete reaction and thus lower reaction efficiency as well as lower photoactivity. The obtained lattice parameters and average crystallite size do not differ much and are gathered in Table 2. However, the lowest lattice parameters and average crystallite size were observed for TiO_2_BPy(1:3), that is for the sample with the highest photocatalytic activity and specific surface area. Analogously, Górska [30] and Cybula [31] also observed the highest photoactivity for TiO_2 samples that had the smallest crystallite size, therefore the highest surface area. Moreover, comparison TiO_2_BPy(1:3) with IL-TiO_2

samples prepared in a presence of various ILs [12, 27] revealed that TiO_2_BPy(1:3) had lower crystallite size, thus higher photoactivity.

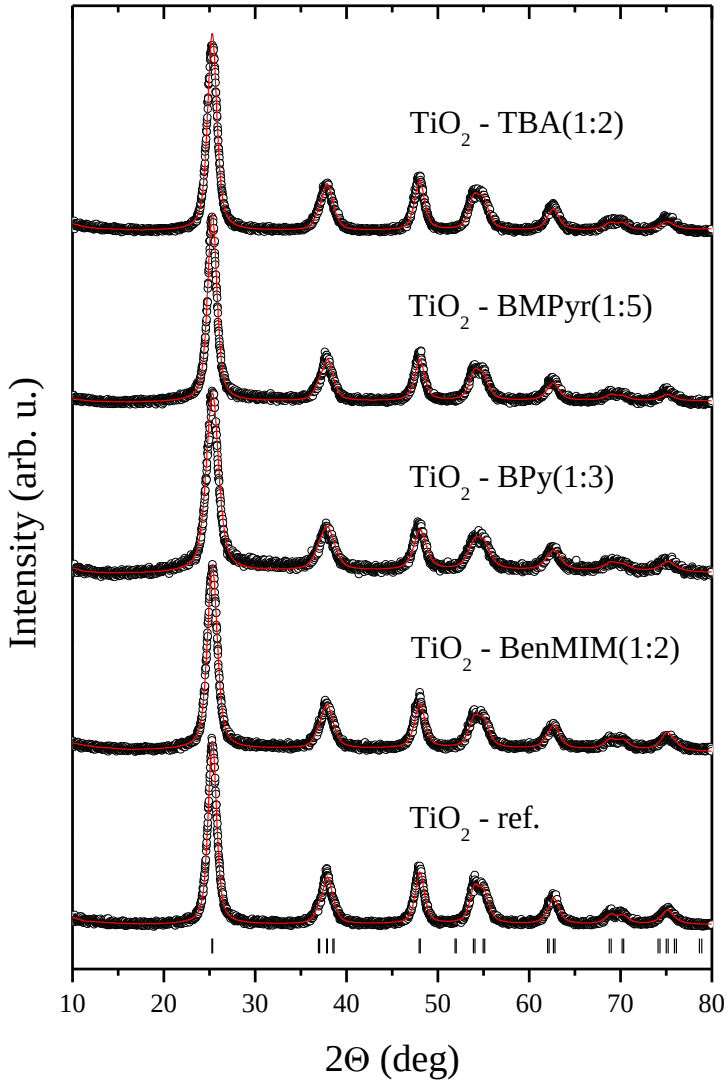

Figure 2. Room temperature powder X-ray diffraction patterns of TiO_2_BenMIM(1:2), TiO_2_BPy(1:3); TiO_2_BMPyr(1:5); TiO_2_TBA(1:2) and reference TiO_2 – anatase. Bragg reflections are represented by black vertical bars, observed and calculated data are shown by black points and a red line, respectively.

Table 2. Lattice parameters and average crystallite size of IL-assisted TiO_2 photocatalysts

Sample label	a (Å)	c (Å)	d (Å)
TiO_2	3.7890(3)	9.497(1)	63
TiO_2_BenMIM(1:2)	3.7889(3)	9.505(1)	54

TiO_2_BPy(1:3)	3.7872(5)	9.494(2)	43
TiO_2_BMPyr(1:5)	3.7907(4)	9.493(2)	57
TiO_2_TBA(1:2)	3.7914(3)	9.506(1)	58

The SEM analysis of four IL-TiO_2 samples with the highest photocatalytic activity (Figure 3) revealed that the particles are spherical with well-developed structure. Application of [TBA][Cl] provided particles with the highest contribution of the smallest fraction, that is 40% of structures had diameters of 0.5-1 µm. It could be the result of fast nucleation rate [32]. The TiO_2 prepared in a presence of [BMPyr][Cl] have relatively more smooth surface and formed bigger structures, 80% particles were in the range of 1-3 µm. However, the photocatalysts obtained with addition of [BenMIM][Cl] and [BPy][Cl] had the most uniform distribution and were composed mainly of particles with diameter ranging from 1 to 2 µm (76%).

The UV-Vis diffuse reflectance spectra (DRS) of the IL-assisted TiO_2 samples were shown in Figure 4. The optical absorption of samples prepared with addition of ILs was shifted to the region of 400-600 nm in comparison to reference TiO_2 characterized by sharp edge detected at 390–400 nm. Interestingly, the highest shift, thus the highest visible light absorption improvement was not observed for the sample with the highest photoactivity, that is TiO_2_BPy(1:3) but for TiO_2_BMPyr(1:5) sample. The significant light absorption of TiO_2_BMPyr(1:5) might be due to the higher content of Ti^{3+} [33]. Analogous observation, namely that optical properties do not go side by side with photocatalytic activity, was already presented in literature for diverse metal and nitrogen codoped TiO_2 photocatalysts [33-37]. The proposed formation mechanism of IL-TiO_2 spheres was already discussed and schematically presented in our previous papers [12, 38].

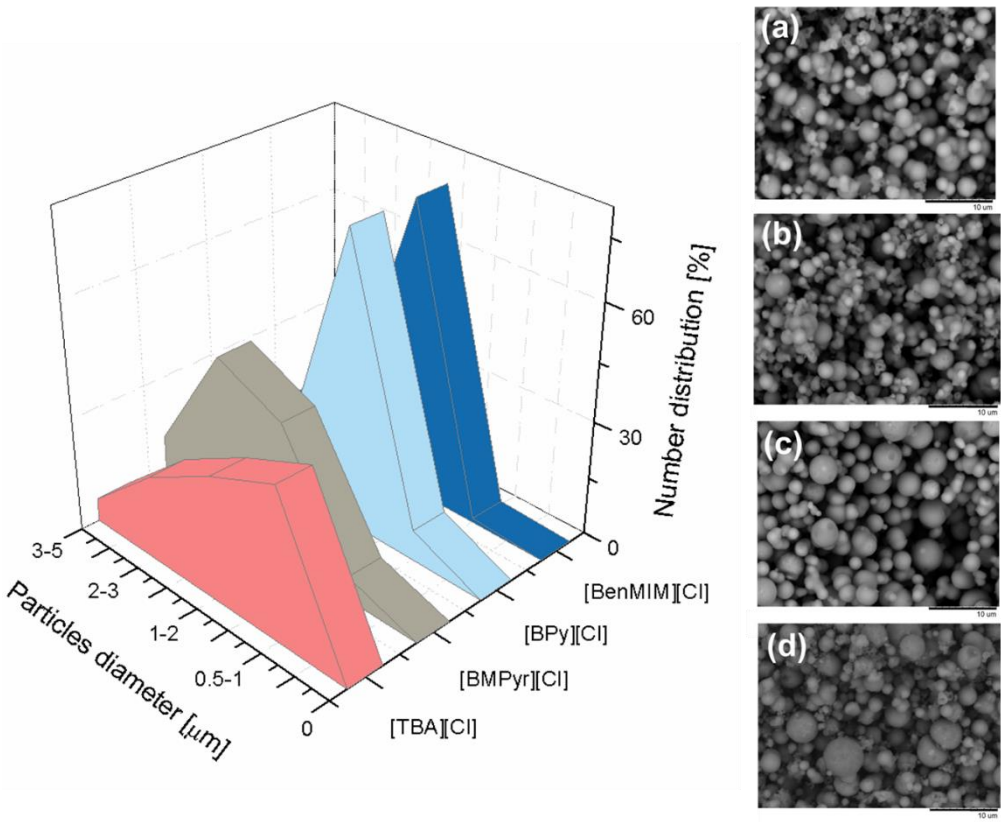

Figure 3. SEM images and particle size distribution of TiO_2 obtained by IL-assisted solvothermal process (a) TiO_2_BenMIM(1:2), (b) TiO_2_BPy(1:3); (c) TiO_2_BMPyr(1:5); (d) TiO_2_TBA(1:2)

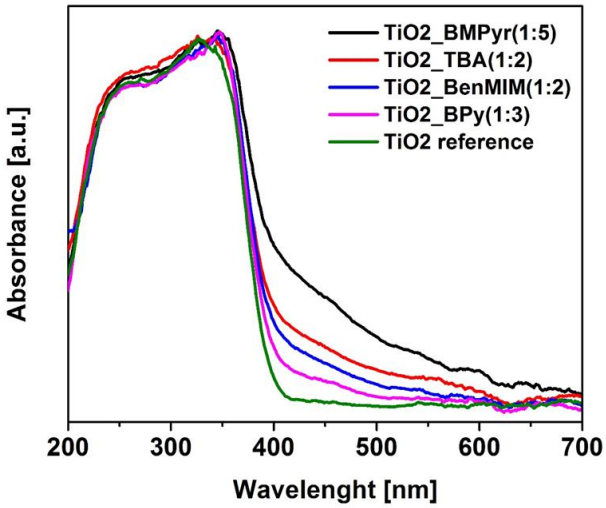

Figure 4. UV-Vis absorption spectra of the ILs-TiO_2 samples and reference TiO_2

4.3 Elemental composition of the IL-assisted samples

The selected ILs-TiO_2 samples, representing the highest photocatalytic activity in each IL-series, were analyzed using XPS. Both the elemental surface composition and chemical character of detected elements were identified [39] in the high-resolution (HR) XPS spectra recorded for each sample. The results are presented in Figure 5 and Table 3. The N 1s and Cl 2p XPS spectra revealed the successful IL modification of the TiO_2 photocatalysts. Nitrogen was detected on all samples in two forms at BE close to 400 eV and 397.5 eV. Fist one identify well the surface IL adspecies formation (C-NH-C, C=N-C bonds, Figure 5) [12, 39] and second evidences the IL interaction with TiO_2 matrix (Ti-Nx bonds, Figure 5) [39-41]. The chemical character of titanium, oxygen and carbon originated from ILs-TiO_2 samples is identified in deconvoluted XPS spectra of Ti 2p, O 1s and C 1s, respectively (Figure 5) and specified in Table 3. The inspection of XPS data collected in Table 3 revealed the relative surface contribution of all detected elements. The atomic concentration (AC) ratios N/Ti, evaluated for TiO_2_BPy (1:3) and TiO_2_BMPyr (1:5) confirm the smaller IL amount in these samples to compare with the TiO_2_BenMIM(1:2) and TiO_2_TBA (1:2) samples. From the other hand, the C/Ti ratio, estimated for the first two samples were found to be much larger than for the last two samples. Since the preparation processing was similar for all samples we can address these data to the partial decomposition of cationic IL surface species in TiO_2_BPy(1:3) and TiO_2_BMPyr(1:5) samples and interaction of nitrogen atoms with deeper sites of TiO_2. This supposition is well confirmed by relatively larger contribution of Ti-Nx species revealed in deconvoluted N1s spectra for these samples (Figure 5). Moreover the C/N values evaluated for TiO_2_BPy(1:3) and TiO_2_BMPyr(1:5) samples (150.7 and 117.7, respectively) are much larger than their nominal IL stoichiometry (9 for both samples). In contrary, the TiO_2_BenMIM(1:2) and TiO_2_TBA(1:2) samples seems more stable and exhibit the C/N values 11.0 and 16.7 and nominal C/N 5.5 and 16.0, respectively (Table 3). The large contributions of surface oxide fractions and carbon species identified in “A” and “B” fractions of C 1s spectra (Figure 5, Table 3) seems to confirm co-adsorption of partially decomposed IL on TiO_2_BPy(1:3) and TiO_2_BMPyr(1:5) samples. These observations corroborates previous studies on thermal stability of ILs that imidazolium derivatives are generally more stable than

tetraalkylammonium-, piperidinium-, and pyridinium-based salts [42], and pyridinium cations are less stable than pyrrolidinum cations [43]. It is also interesting to note that the relative amount of the Ti^{3+} ions in these samples is about twice bigger than for TiO_2_BenMIM(1:2) and TiO_2_TBA(1:2) samples with larger IL contents (Table 2). In this regard, the higher Ti^{3+} content accompanied by relatively larger contribution of Ti-Nx species may explain higher photocatalytic activity of TiO_2_BPy(1:3) and TiO_2_BMPyr(1:5).
Results obtained by XPS method were also confirmed by CHNS measurements (Figure S1). The CHNS analysis also revealed the presence of carbon, nitrogen and hydrogen atoms in the compositions of the IL-TiO_2, thus confirmed presence of the elements characteristic for ILs used in this study. The carbon, hydrogen and nitrogen peaks may be attributed to the residual IL and decomposition products present at the surface of the TiO_2 particles as well as doping of the TiO_2 with nitrogen.

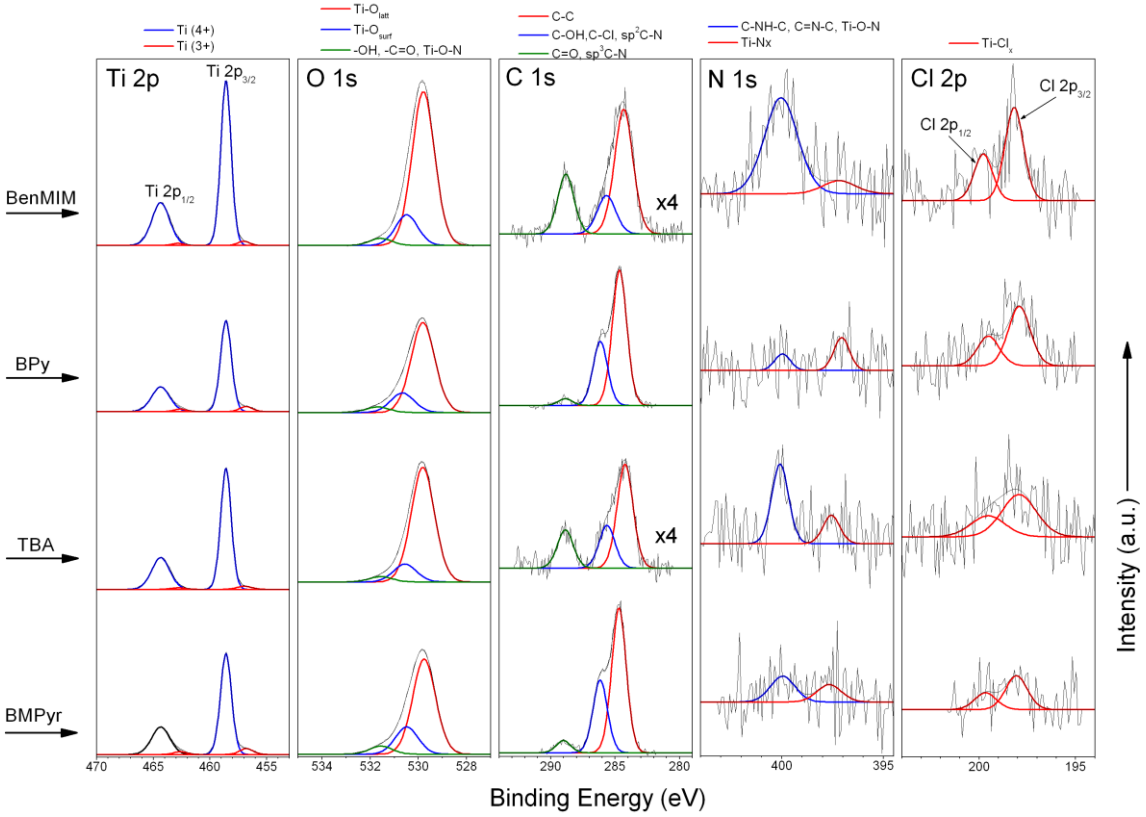

Figure 5. XPS HR spectra Ti 2p, O 1s, C 1s, N 1s, Cl 2p of ionic liquid-assisted TiO_2 photocatalysts

Table 3. Elemental composition (in at. %) and chemical characters of titanium, oxygen and carbon states in the surface layer of [BenMIM][Cl]-, [BPy][Cl]-, [TBA][Cl]- and [BMPyr][Cl]-modified TiO_2 particles, evaluated by XPS analysis

Sample	Ti fraction (%)			O fraction (%)				C fraction (%)				∑ N (at.%)	∑ Cl (at.%)	C/N	N/Ti	Cl/Ti	Cl/N
	∑ Ti (at.%)	Ti(4+) 458.6 eV	Ti(3+) 456.9±0.1 eV	∑ O (at.%)	Ti-O_{latt} 529.8 eV	Ti-O_{surf} 530.6±0.1 eV	-OH,-C=O, Ti-O-N, 531.7±0.1 eV	∑ C (at.%)	"A" C-C 284.6±0.2 eV	"B" C-OH, C-Cl sp^2C-N 285.9±0.3 eV	"C" -C=O, sp^3C-N 288.9±0.1 eV						
TiO_2_BenMIM(1:2)	29.92	97.00	3.00	67.22	80.22	16.00	3.78	2.52	57.86	17.86	24.28	0.23	0.11	11.0	0.0077	0.0037	0.48
TiO_2_BPy (1:3)	26.80	93.34	6.66	62.44	78.10	16.90	5.00	10.55	65.62	31.11	3.27	0.07	0.12	150.7	0.0026	0.0045	1.71
TiO_2_TBA (1:2)	30.26	96.14	3,86	66.97	83.03	12.99	3.98	2.51	56.15	23.13	20.72	0.15	0.12	16.7	0.0050	0.0040	0.80
TiO_2_BMPyr(1:5)	27.24	92.73	7.27	62.01	72.78	20.91	6.32	10.59	62.92	31.72	5.35	0.09	0.06	117.7	0.0033	0.0022	0.67

4.4 Determination of reactive species

The trapping experiments were conducted to reveal the active species role in the phenol degradation process under Vis irradiation using the IL-TiO_2 sample with the highest activity, that was TiO2_BPy(1:3). Four different scavengers were used: ammonium oxalate as a scavenger of photogenerated holes (h^+), $AgNO_3$ for electrons (e^-), benzoquinone for superoxide radical species ($O_2^{\bullet-}$), and tert-butyl alcohol for hydroxyl radical species (•OH). As it was shown in Figure 6, benzoquinone was a scavenger that inhibited the phenol photodegradation with the highest efficiency that means that $O_2^{\bullet-}$ were main active species responsible for high efficiency of degradation.

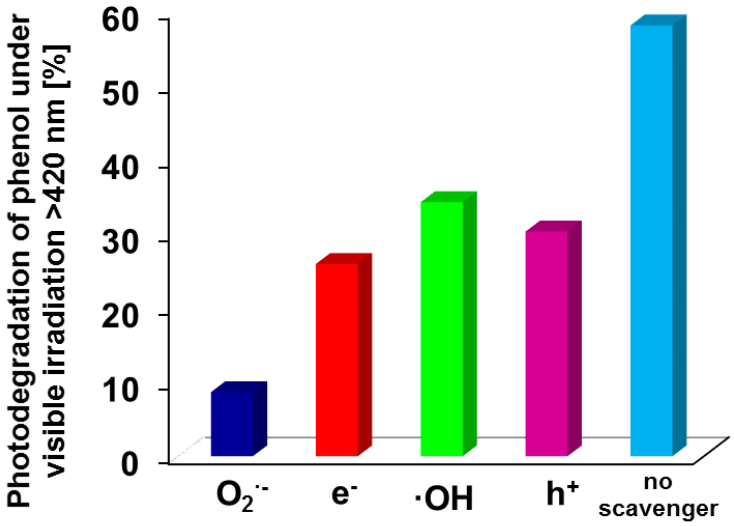

Figure 6. Efficiency of phenol degradation in the presence of the TiO2_BPy(1:3) sample and different scavengers after 60 min of visible light irradiation

The effect of the use of ILs in the preparation of titania-based systems has also been evaluated investigating the photoactivity of the new materials by Electron Paramagnetic Resonance. This has been done monitoring the photoinduced electron transfer from the solid to molecular oxygen in the gas phase with formation of the paramagnetic superoxide species, O_2^-, which becomes adsorbed at the surface. In ~~the~~ a first step, the experiments of irradiation samples were done in vacuum in order to see if charge separation occurs. In this case the irradiation leads to promotion of an electron (e–) in the conduction band (CB) and the formation of an electron hole (or hole, h^+) in the valence band (VB):

$$TiO_2 + h\nu \rightarrow e^-_{(CB)} + h^+_{(VB)}$$

If the charge carries are not transferred to other molecules, the electrons are trapped by Ti^{4+} forming Ti^{3+} ($Ti^{4+} + e^-_{(CB)} \rightarrow Ti^{3+}$). Next, to check the capability of the photogenerated charge to reach the surface of the nanoparticles, irradiation of samples was performed ~~in the~~ under oxygen atmosphere. The gas phase O_2 molecule, indeed, reacts with those photogenerated electrons capable of reaching the surface, producing surface adsorbed superoxide O_2^- :

$$e^-_{(CB)} + O_{2\,(gas)} + Ti^{4+}_{(surf)} \rightarrow O_2^{-}\cdots Ti^{4+}_{(surf)}$$

~~($Ti^{3+} + e^- \rightarrow Ti^{4+} + O_2^-$).~~ For this reason, in the EPR spectra performed upon irradiation under oxygen atmosphere, superoxide species only are observed (and not Ti^{3+} ions) ~~are not noticeable observed but only~~ (Figure 7). The effect of both visible light (cut off of the lamp at 420 nm) and polychromatic UV-Vis (full lamp) on the various materials has been followed and the results are

reported in Figure 7. The EPR spectrum of reference TiO_2 recorded in dark conditions (Figure 7a) shows a nearly flat base line with a barely visible absorption due to tiny amounts of defects. Interestingly, under visible light irradiation the observed EPR signals of the two IL-TiO_2 composite materials (Figure 7c and 7d) are typical of superoxide ions on titania whose spectral features are widely described elsewhere. ~~The superoxides are formed since electrons are scavenged by oxygen which reduces to superoxide and adsorbs onto surface Ti^{4+} ions at the surface ($O_2 + e^-_{CB} \rightarrow O_2^-_{(surf)}$)~~. Pristine TiO_2 (Figure 7b), in turn, is practically incapable to form superoxide due to the fact that the frequency of the visible range do not cover the band gap value. The amount of superoxide ions formed by the effect of visible light is smaller than that formed *via* UV irradiation (as indicated by comparison of the intensity of the two groups of spectra in Figure 7 namely b, c, d vs. e, f, g) but is definitely appreciable and not negligible. The EPR spectra in Figure 7 thus confirm that the use of ILs in the preparation procedure causes a sensitization of the samples to the visible light. The materials prepared in this way are capable to use visible photons beside UV ones for the promotion of electrons in the conduction band similarly to what previously observed for nitrogen doped and nitrogen-fluorine co-doped materials prepared by different synthetic routes [44]. ~~Performed for comparison experiments with in the presence of gaseous oxygen also results in. This~~ The formation of surface adsorbed O_2^- under UV-vis light (Figure 7e-g) occurs because of the excitation of valence band electron to the conduction band induced by the UV components of the irradiation capable to cover the band gap energy that is about 3.2 eV for anatase [45]. As it is possible to observe from the EPR spectra, the effect of UV light on the samples is similar in the three different cases ~~and generates the formation of superoxide species~~ (signals 7 e, f, g). The presence of IL does not hamper the formation of superoxide under UV irradiation that is slightly reduced in the case of the TiO_2_BMPy 1:2 sample (7g) with respect to the bare titania (7e) while in the case of TiO_2_BPy 1:3 (7f) the electron transfer capability is unaffected.

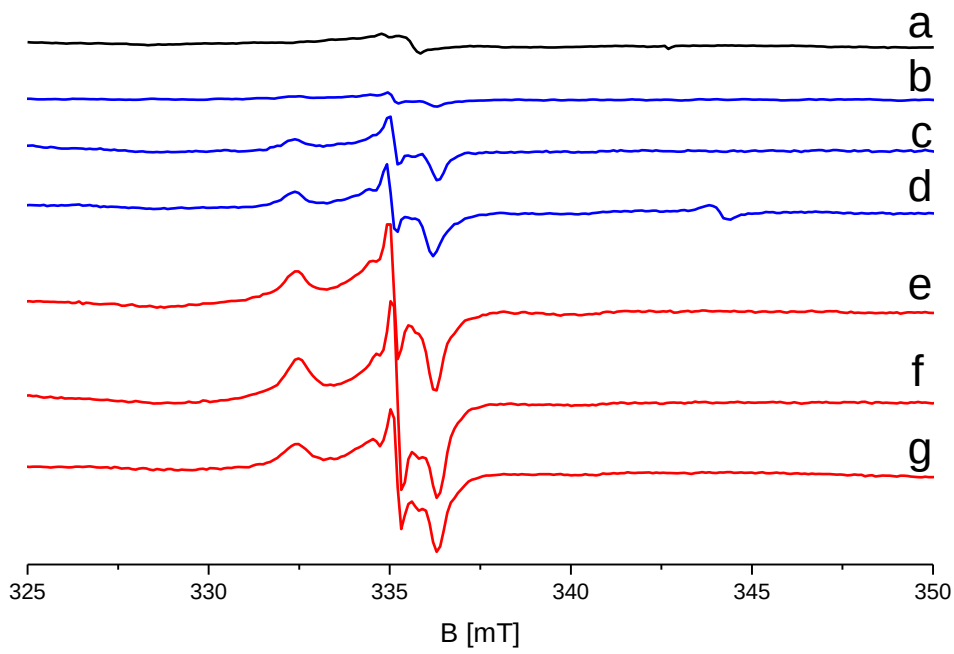

Figure 7. EPR spectra of a) reference TiO_2 recorded in dark; b-d) materials irradiated under O_2 with visible light (λ > 420 nm). b) TiO_2, c) TiO_2_BPy 1:3 and d) TiO_2_BMPy 1:2. e-g) materials irradiated under O_2 with UV and visible light (full lamp): e) TiO_2, f) TiO_2_BPy 1:3, g) TiO_2_BMPy 1:2

Further recognition of the photoactivity process was performed by determination of the recombination of the photogenerated electrons and holes by photoluminescence method (PL). The steady-state PL spectra of as-prepared IL-TiO_2 photocatalysts revealed an emission band in the wavelength range of 350–550 nm, which was assigned to the excitonic band edge emission of TiO_2. The TiO_2 photocatalysts had a weak PL maximum at 395 nm (3.14 eV) which corresponds to recombination of photoinduced band-gap electrons and holes. As show four characteristic peaks at 451 nm, 468 nm, 483 nm, and 493 nm appear in the PL spectra, which mainly resulted from surface oxygen vacancies and defects in the samples. The FL peaks at 451 and 468 nm are attributed to band edge free excitons, and the other two peaks at 483 and 493 nm are attributed to bound excitons. These features are considered to be a kind of intrinsic defects in TiO_2 lattice forming intermediate energy levels [46]. It is known that the lower the PL intensity means the higher separation efficiency of electron-hole pairs. As shown in Figure 8 the intensity of photoluminescence of most IL-TiO_2 particles is lower than that of pure TiO_2, implying that the presence of ILs could effectively improves the inhibition of electron and electron-hole recombination. However, samples that exhibited the lowest PL signal were not the most active ones.

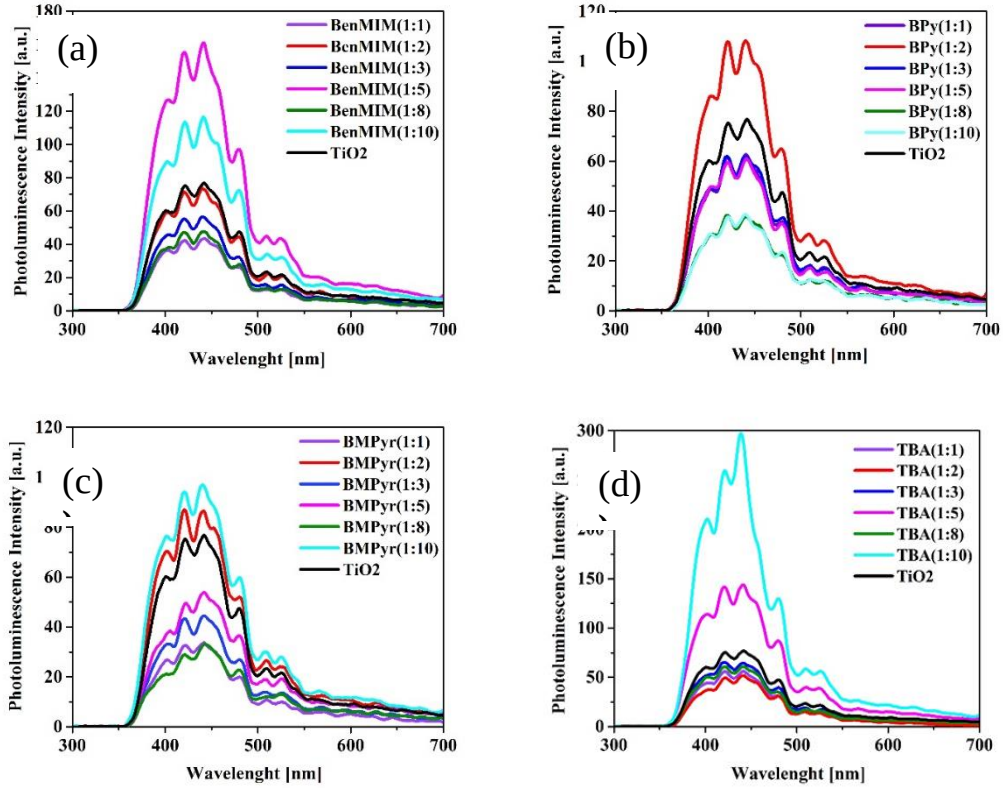

Figure 8. Photoluminescence spectra of samples prepared by IL-assisted solvothermal method in the presence of: (a) [BenMIM][Cl]; (b) [BPy][Cl]; (c) [BMPyr][Cl]; (d) [TBA][Cl] and reference TiO_2 particles

4.5 Discussion of photocatalytic activity

The sample that reveled the highest photocatalytic activity under Vis light (58% of phenol degradation after 1h irradiation) was TiO_2_BPy(1:3), that is TiO_2 obtained in a presence of [BPy][Cl] ionic liquid at 1 to 3 IL:TBOT molar ratio. Moreover, this sample had also the most uniform distribution (76% of particles had diameter in the range of 1 to 2 μm), the lowest lattice

parameters (a = 3.7872(5) Å, c = 9.494(2) Å) and average crystallite size (43 nm), hence the largest surface area (215 $m^2 g^{-1}$). This properties resulted in more active sites that shorten the bulk diffusion length of charge carriers and suppress their recombination, thus resulted in higher photoactivity [47]. The TiO_2_BPy(1:3) sample consisted of 26.80 at.% of Ti (6.66 at.% of which were Ti^{3+}), 62.44 at.% of O, 10.55 at.% of C, 0.07 at.% of N and 0.12 at.% of Cl. As has been shown previously (based on the XPS measurements) the partial decomposition of cations of ILs takes place. Decomposition of [BPy][Cl] and [BMPyr][Cl] takes part with the relatively higher extend in comparison with other ILs resulting in co-adsorption of partially decomposed IL at the TiO_2 surface and larger contribution of interaction of nitrogen atoms with deeper sites of TiO_2 and formation of Ti-Nx species. Up to now, nitrogen doping is regarded as one of the most effective approaches to extend the absorption edge of TiO_2 which enhances its photocatalytic activity under visible light irradiation because of its comparable atomic size with oxygen, small ionization energy, metastable center formation, and stability. It results in the change of the banding structure of TiO_2 due to the N interstitial doping, N-substitution, and the formation of surface oxygen vacancies which cause the red-shift absorption edge of TiO_2 [48-50]. Indeed, shift the optical absorption to the visible light region for all IL-TiO_2 was observed. In this regard, the proposed photocatalytic mechanism for the obtained samples under Vis irradiation was shown in Figure 9. With the induction of N into TiO_2 lattice, new impurity level including the N 2p above the O 2p valence band could be formed. Wang et al explained that the valence band position of the N-doped TiO_2 does not shift upward due to interstitial N-doping in spite of formation of the N 2p surface state [51]. Electrons on this N 2p surface state would transit to the conduction band of the TiO_2 upon absorption of light in longer wavelength, resulting in enhanced absorption of TiO_2 on visible light [51]. As a consequence, electrons can be transferred from the N 2p surface state to the conduction band leading to the formation of electron and hole pairs. Finally electrons accumulated at the surface of photocatalysts could be scavenged by oxygen molecules resulting in formation of highly oxidative species [52]. It is also worth to mention that the relative amount of the Ti^{3+} ions in the TiO_2_BPy(1:3) sample is about twice higher than for the TiO_2_BenMIM(1:2) and TiO_2_TBA(1:2) samples, although the molar ratio of IL to TBOT used for synthesis was higher (see details in Table 3). In this regard, the presence of Ti^{3+} can introduce impurity states below the conduction band [53]. Taking into consideration the bandgap modification both by the presence of Ti^{3+} and N-doping, it is supposed that the interaction between Ti^{3+} and N is responsible for the red shift of absorption edge and high phenol photo-oxidation performance of TiO_2 under visible light irradiation. Electrons from conduction band or Ti^{3+} state could react with oxygen molecules providing oxidative species such as superoxide radical anions, being the main active species responsible for high efficiency of photodegradation. In the meantime, the holes that are generated in the valence band or N-dopant levels could react with hydroxyl anions or water providing hydroxyl radicals. In view of this, the Ti^{3+} content accompanied by contribution of Ti-Nx species may reduce the photon excitation energy from the VB to the CB under visible-light irradiation, thus explain enhanced photocatalytic activity of these samples in these conditions.

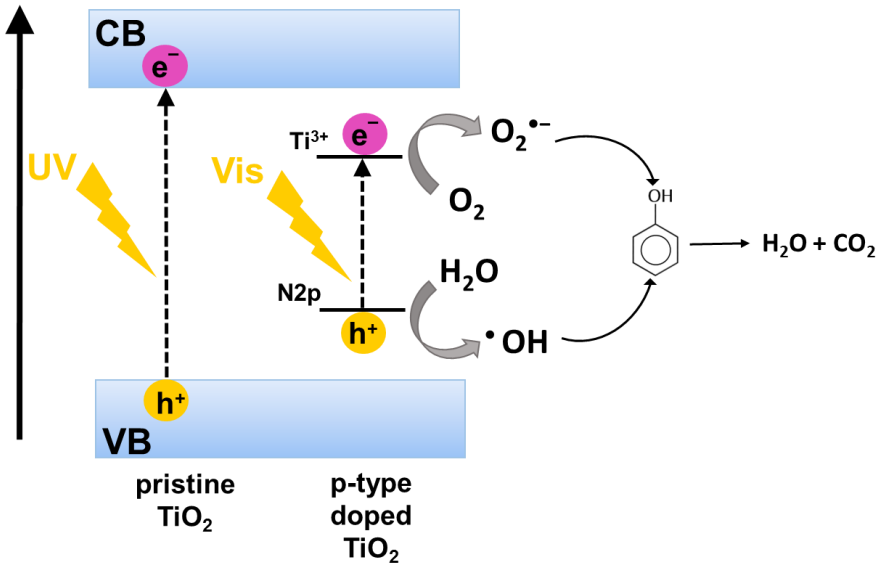

Figure 9. Proposed photocatalytic mechanism over IL-TiO_2 under visible light irradiation

5. Conclusions

Highly active under visible light IL-TiO_2 composites were obtained through simple ionic liquid assisted-solvothermal synthesis method using ILs composed of distinct, nitrogen containing, cations and chloride anions. The photoactivity of the IL-TiO_2 particles was found to be highly dependent on the amount of IL (molar ratio of TBOT:IL) used for synthesis and significantly differed for various IL structures. To high IL content results in overloading of the TiO_2 surface with IL, thus decrease of specific surface area and photoactivity. In this regard we revealed that preparation of IL-TiO_2 have to be preceded by careful selection not only the IL's structure but also its content since it strongly determines the morphological feature as well as photoactive properties of the IL-semiconductor composite. Unfortunately, in most publications this parameter is omitted when the IL-TiO_2 properties are characterized.

The highest degradation efficiency of phenol (selected as model pollution) under Vis irradiation, that is 58%, was revealed for TiO_2 sample obtained in a presence of 1-butylpyridinium chloride [BPy][Cl]. This sample had the lowest lattice parameters, average crystallite size, the highest specific surface area, and the most uniform distribution. Moreover, the relative amount of the Ti^{3+} defects in this sample was found to be about twice higher than in IL-TiO_2 samples prepared in a presence of ammonium and imidazolium derivatives prepared with larger IL contents (providing the highest photoactivity for specific IL).

It was also revealed that in the selected TiO_2 preparation route ionic liquids served not only as a structural agent but also as a surface modifier and source of nitrogen incorporated into the TiO_2 structure (Ti-Nx bonds). Therefore, the IL-TiO_2 photocatalysts were found to be capable to use visible photons beside UV ones for the promotion of electrons in the conduction band (or Ti^{3+} state) similarly to what was previously observed for nitrogen doped materials prepared by different synthetic methods. Moreover, the photocatalytic activity under Vis irradiation was found to be attributable mainly to $O_2^{\bullet-}$, however other forms of reactive oxygen species, such as •OH, H_2O_2 and $HO_2^{\bullet}$ radicals were also involved in the phenol degradation process.

These comparative studies give us better phenomenological insight into the performance of IL-TiO_2 photocatalysts and better prospects for optimizing reaction components of choice. They are a part of a very broad, but almost untouched issue in the field of IL-TiO_2 composites, namely which structural descriptors of ILs are crucial for preparation of photocatalyst with desired morphology

and properties and to how to predict the properties of IL-TiO_2 materials on the basis of the structure and properties of ionic liquids. The Authors hope that results presented here will stimulate further studies designed to increase the photoactivity of TiO_2 as well as better understanding of IL's role in mechanism of heterogenous photocatalysis, therefore influence the potential for commercial application.

6. References

[1] A. Fujishima, T.N. Rao, D.A. Tryk, Titanium dioxide photocatalysis, Journal of Photochemistry and Photobiology C: Photochemistry Reviews, 1 (2000) 1-21.

[2] B. Ohtani, Photocatalysis A to Z—What we know and what we do notknow in a scientific sense, Journal of Photochemistry and Photobiology C: Photochemistry Reviews 11 (2010) 157–178.

[3] K. Nakata, A. Fujishima, TiO2 photocatalysis: Design and applications, Journal of Photochemistry and Photobiology C: Photochemistry Reviews, 13 (2012) 169-189.

[4] Y. Yu, Y. Jiang, M. Tian, L. Yang, H. Yan, S. Sheng, N-Doped TiO 2 Nanotube Arrays: Synthesis by Anodization in an Ionic Liquid ([BMIM] BF 4) and Assessment of Photocatalytic Property, Rare Metal Materials and Engineering, 45 (2016) 561-566.

[5] S. Yu, B. Liu, Q. Wang, Y. Gao, Y. Shi, X. Feng, X. An, L. Liu, J. Zhang, Ionic Liquid Assisted Chemical Strategy to TiO2 Hollow Nanocube Assemblies with Surface-Fluorination and Nitridation and High Energy Crystal Facet Exposure for Enhanced Photocatalysis, ACS applied materials & interfaces, 6 (2014) 10283-10295.

[6] S. Hu, H. Wang, J. Cao, J. Liu, B. Fang, M. Zheng, G. Ji, F. Zhang, Z. Yang, Synthesis of mesostructure anatase TiO2 particles in room-temperature ionic liquids, Materials Letters, 62 (2008) 2954–2956.

[7] R. Ramanathan, V. Bansal, Ionic liquid mediated synthesis of nitrogen, carbon and fluorine-codoped rutile TiO2 nanorods for improved UV and visible light photocatalysis, RSC Advances, 5 (2015) 1424-1429.

[8] K. Yoo, H. Choi, D. Dionysiou, Ionic liquid assisted preparation of nanostructured TiO2 particles, Chemical Communications, (2004) 2000–2001.

[9] S. Chang, C. Lee, A salt-assisted approach for the pore-size-tailoring of the ionic-liquid-templatedTiO2 photocatalysts exhibiting high activity, Applied Catalysis B: Environmental, 132-133 (2013) 219– 228.

[10] F. Mirhoseini, A. Salabat Ionic liquid based microemulsion method for the fabrication of poly(methyl methacrylate)–TiO_2nanocomposite as a highly efficient visible light photocatalyst, RSC Advances, 5 (2015) 12536-12545.

[11] B. Wang, L. Guo, M. Hea, T. He, Green synthesis of TiO2 nanocrystals with improved photocatalytic activity by ionic-liquid assisted hydrothermal method, Physical Chemistry Chemical Physics, 15 (2013) 9891 - 9898.

[12] M. Paszkiewicz, J. Łuczak, W. Lisowski, P. Patyk, A. Zaleska-Medynska, The ILs-assisted solvothermal synthesis of TiO2 spheres: The effect of ionic liquids on morphology and photoactivity of TiO2, Applied Catalysis B: Environmental, 184 (2016) 223-237.

[13] A. Suzuki, H. Yamaguchi, H. Kageyama, O. Yuya, Microwave-assisted rapid synthesis of anatase TiO2 nanosized particles in an ionic liquid-water system, Journal of the Ceramic Society of Japan, 123 (2015) 79-82.

[14] X. Wang, F. Li, J. Liu, C. Kou, X. Zhao, Y. Hao, D. Zhao, Preparation of TiO2 in Ionic Liquid via Microwave Radiation and in Situ Photocatalytic Oxidative Desulfurization of Diesel Oil, Energy Fuels, 26 (2012) 6777−6782.

[15] K. Ding, Z. Miao, Z. Liu, Z. Zhang, B. Han, G. An, S. Miao, Y. Xie, Facile Synthesis of High Quality TiO2 Nanocrystals in Ionic Liquid via a Microwave-Assisted Process, Journal of the American Chemical Society, 129 (2007) 6362-6363.
[16] Y. Chen, W. Li, J. Wang, Y. Gan, L. Liu, M. Ju, Microwave-assisted ionic liquid synthesis of Ti3+ self-doped TiO2 hollow nanocrystals with enhanced visible-light photoactivity, Applied Catalysis B: Environmental, 191 (2016) 94-105.
[17] J. Łuczak, M. Paszkiewicz, A. Krukowska, A. Malankowska, A. Zaleska-Medynska, Ionic liquids for nano- and microstructures preparation. Part 2: Application in synthesis, Advances in Colloid and Interface Science, 227 (2016) 1-52.
[18] J. Łuczak, M. Paszkiewicz, A. Krukowska, A. Malankowska, A. Zaleska-Medynska, Ionic liquids for nano- and microstructures preparation. Part 1: Properties and multifunctional role, 230 (2016) 13–28.
[19] J. Łuczak, J. Hupka, J. Thöming, C. Jungnickel, Self-organization of imidazolium ionic liquids in aqueous solution, Colloids and Surfaces A: Physicochemical and Engineering Aspects, 329 (2008) 125–133.
[20] C. Han, S. Ho, Y. Lin, Y. Lai, W. Liang, Y. Chen-Yang, Effect of p–p stacking of water miscible ionic liquid template with different cation chain length and content on morphology of mesoporous TiO2 prepared
via sol–gel method and the applications, Microporous and Mesoporous Materials, (2010) 217–223.
[21] S. Hu, A. Wang, X. Li, Y. Wang, H. Löwe, Hydrothermal Synthesis of Ionic Liquid [Bmim] OH-Modified TiO2 Nanoparticles with Enhanced Photocatalytic Activity under Visible Light, Chemistry–An Asian Journal, 5 (2010) 1171-1177.
[22] J.L. Junbo Zhong, Famei Feng, Shengtiang Huang,, C.B. Weidong Jiang, Ionic Liquid-Assisted Fabrication of Nanoscale Microporous TiO_2 with Enhanced Photocatalytic Performance, JSM Nanotechnol Nanomed, 1(2) (2013) 1-6.
[23] L. Jing, M. Wang, X. Li, R. Xiao, Y. Zhao, Y. Zhang, Y.-M. Yan, Q. Wu, K. Sun, Covalently functionalized TiO 2 with ionic liquid: A high-performance catalyst for photoelectrochemical water oxidation, Applied Catalysis B: Environmental, 166 (2015) 270-276.
[24] L. Qi, J. Yu, M. Jaroniec, Enhanced and suppressed effects of ionic liquid on the photocatalytic activity of TiO2, Adsorption, 19 (2013) 557-561.
[25] J. Yu, Q. Li, S. Liu, M. Jaroniec, Ionic-Liquid-Assisted Synthesis of Uniform Fluorinated B/C-Codoped TiO2 Nanocrystals and Their Enhanced Visible-Light Photocatalytic Activity, Chemistry - A European Journal, 19 (2013) 2433 – 2441.
[26] P. Mazierski , J. Łuczak , W. Lisowski , M.J. Winiarski , T. Klimczuk , A. Zaleska-Medynska T**he ILs-assisted electrochemical synthesis of** T**iO2 nanotubes: the effect of ionic liquids on morphology and photoactivity**The ILs-assisted electrochemical synthesis of TiO2 nanotubes: the effect of ionic liquids on morphology and photoactivity, Applied Catalysis B: Environmental, https://doi.org/10.1016/j.apcatb.2017.05.005 (2017).
[27] J. Łuczak , M. Paszkiewicz-Gawron , M. Długokęcka , W. Lisowski , E. Grabowska , S. Makurat, J. Rak, A. Zaleska-Medynska **[BMIM][X]-assisted (X = Br, PF6, OctSO4) solvothermal synthesis of TiO2 particles: effect of the ionic liquid's anion on the morphology and photoactivity of TiO2**Visible light photocatalytic activity of ionic liquid-TiO2 spheres: effect of the ionic liquid's anion structure, ChemCatChem, in review (2017).
[28] X. Yan, T. Ohno, K. Nishijima, R. Abe, B. Ohtani, Is methylene blue an appropriate substrate for a photocatalytic activity test? A study with visible-light responsive titania Chemical Physics Letters, 429 (2006) 606–610.

[29] F. Li, X. Wang, Y. Zhao, J. Liu, Y. Hao, R. Liu, D. Zhao, Ionic-liquid-assisted synthesis of high-visible-light-activated N–B–F-tri-doped mesoporous TiO2 via a microwave route, 144 (2014) 442–453.
[30] P. Górska, A. Zaleska, E. Kowalska, T. Klimczuk, J.W. Sobczak, E. Skwarek, W. Janusz, J. Hupka, TiO2 photoactivity in Vis and UV light: The influence of calcination temperature and surface properties, Applied Catalysis B: Environmental, 84 (2008) 440-447.
[31] A. Cybula, J.B. Priebe, M.-M. Pohl, J.W. Sobczak, M. Schneider, A. Zielińska-Jurek, A. Brückner, A. Zaleska, The effect of calcination temperature on structure and photocatalytic properties of Au/Pd nanoparticles supported on TiO2, Applied Catalysis B: Environmental, 152–153 (2014) 202-211.
[32] A. Baldan, Progress in Ostwald ripening theories and their applications to nickel-base superalloys Part I: O*stwald ripening theories*, Journal of Materials Science, 37 (2002) 2171-2202.
[33] C.-C. Pan, J.C.S. Wu, Visible-light response Cr-doped TiO2−XNX photocatalysts, Materials Chemistry and Physics, 100 (2006) 102-107.
[34] C. Liu, X. Tang, C. Mo, Z. Qiang, Characterization and activity of visible-light-driven TiO2 photocatalyst codoped with nitrogen and cerium, Journal of Solid State Chemistry, 181 (2008) 913-919.
[35] S. Hu, F. Li, Z. Fan, The influence of preparation method, nitrogen source, and post-treatment on the photocatalytic activity and stability of N-doped TiO2 nanopowder, Journal of Hazardous Materials, 196 (2011) 248-254.
[36] S. Lee, I.-S. Cho, D.K. Lee, D.W. Kim, T.H. Noh, C.H. Kwak, S. Park, K.S. Hong, J.-K. Lee, H.S. Jung, Influence of nitrogen chemical states on photocatalytic activities of nitrogen-doped TiO2 nanoparticles under visible light, Journal of Photochemistry and Photobiology A: Chemistry, 213 (2010) 129-135.
[37] J. Ananpattarachai, P. Kajitvichyanukul, S. Seraphin, Visible light absorption ability and photocatalytic oxidation activity of various interstitial N-doped TiO2 prepared from different nitrogen dopants, Journal of Hazardous Materials, 168 (2009) 253-261.
[38] J. Łuczak , M. Paszkiewicz-Gawron , M. Długokęcka , W. Lisowski , E. Grabowska , S. Makurat, J. Rak, A. Zaleska-Medynska Visible light photocatalytic activity of ionic liquid-TiO2 spheres: effect of the ionic liquid's anion structure, ChemCatChem, in review (2017).
[39] A.V. Naumkin, A. Kraut-Vass, S.W. Gaarenstroom, C.J. Powell, NIST X-ray Photoelectron Spectroscopy Database 20, Version 4.1, 2012.
[40] R. Asahi, T. Morikawa, H. Irie, T. Ohwaki, Nitrogen-doped titanium dioxide as visible-light-sensitive photocatalyst: designs, developments, and prospects, Chemical reviews, 114 (2014) 9824-9852.
[41] R.P. Antony, T. Mathews, K. Panda, B. Sundaravel, S. Dash, A. Tyagi, Enhanced field emission properties of electrochemically synthesized self-aligned nitrogen-doped TiO2 nanotube array thin films, The Journal of Physical Chemistry C, 116 (2012) 16740-16746.
[42] A. Cao, T. Mu, Comprehensive Investigation on the Thermal Stability of 66 Ionic Liquids by Thermogravimetric Analysis, Industrial & Engineering Chemistry Research, 53 (2014) 8651−8664.
[43] E.M. Siedlecka, M. Czerwicka, S. Stolte, P. Stepnowski, Stability of Ionic Liquids in Application Conditions, Current Organic Chemistry, 15 (2011) 1974-1991.
[44] C.D. Valentin, E. Finazzi, G. Pacchioni, A. Selloni, S. Livraghi, A. Czoska, M.C. Paganini, E. Giamello, Density Functional Theory and Electron Paramagnetic Resonance Study on The effect of N-F codoping of TiO2, Chemistry of Materials, 20 (2008) 3706-3714.

[45] G. Barolo, S. Livraghi, M. Chiesa, M.C. Paganini, E. Giamello, Mechanism of the Photoactivity under Visible Light of N-Doped Titanium Dioxide. Charge Carriers Migration in Irradiated N-TiO2 Investigated by Electron Paramagnetic Resonance, Journal of Physical Chemistry C 116 (2012) 20887−20894.
[46] L. Kernazhitsky, V. Shymanovska, T. Gavrilko, V. Naumov, L. Fedorenko, V. Kshnyakin, J. Baran, Room temperature photoluminescence of anatase and rutile TiO 2 powders, Journal of Luminescence, 146 (2014) 199-204.
[47] A.L. Linsebigler, G. Lu, J.T. Yates, Photocatalysis on TiO2 Surfaces: Principles, Mechanisms, and Selected Results, Chemical Reviews, 95 (1995) 735-758.
[48] Z. Jiang, L. Kong, F.S. Alenazey, Y. Qian, L. France, T. Xiao, P.P. Edwards Enhanced visible-light-driven photocatalytic activity of mesoporous $TiO2_{-xN}$xderived from the ethylenediamine-based complex, Nanoscale, 5 (2013) 5396-5402.
[49] T.C. Jagadale , S.P. Takale , R.S. Sonawane , H.M. Joshi , S.I. Patil , B.B. Kale, S.B. Ogale, N-Doped TiO2 Nanoparticle Based Visible Light Photocatalyst by Modified Peroxide Sol−Gel Method Journal of Physical Chemistry B, (2008) 14595–14602.
[50] S. Hu, A. Wang, X. Li, H. Löwe, Hydrothermal synthesis of well-dispersed ultrafine N-doped TiO2nanoparticles with enhanced photocatalytic activity under visible lightJ, Journal of Physics and Chemistry of Solids, 71 (2010) 156–162.
[51] Y. Wang, L. Zhu, N. Ba, Xie, H.,, Effects of NH 4 F quantity on N-doping level, photodegradation and photocatalytic H 2 production activities of N-doped TiO 2 nanotube array films, Materials Research Bulletin, 86 (2017) **268–276**.
[52] S.A. Ansari , M.M. Khan, M.O. Ansari, M.H. Cho, Nitrogen-doped titanium dioxide (N-doped TiO 2) for visible light photocatalysis, New Journal of Chemistry, 146 (2016) 199–204.
[53] W. Fang, M. Xing, J. Zhang, Modifications on reduced titanium dioxide photocatalysts: A review, Journal of Photochemistry and Photobiology C: Photochemistry 32 (2017) 21–39.